Electronic Supplementary Material (ESI) for Sustainable Energy & Fuels.
This journal is © The Royal Society of Chemistry 2020

Primary graphitization of multi-functional dihydropyridine, a novel way to reconstruct TiO_2 surface to obtain high photocatalytic activity for hydrogen peroxide synthesis

Suyan Li,[a] Xiaoyu Hu,[a] Yubo Li,[a] Yu Chen,[a,b] Manman Mu,[a] Lijun Zhang[a,b,*]

[a] School of Chemistry and Chemical Engineering, Tianjin University of Technology, Tianjin 300384, PR China

[b] Tianjin Key Laboratory of Organic Solar Cells and Photochemical Conversion, Tianjin University of Technology, Tianjin 300384, PR China

*Corresponding author at: 391 Binshui West Road, Xiqing District, Tianjin, 300384, PR China. Tel.: +86 02260214258; fax: +86 02260214252. E-mail addresses: cdlijun2002@tjut.edu.cn.

Index

1 Characterization

1.1 Detailed process for photoelectrochemical characterizations

Photoelectrochemical characterizations were conducted on a conventional three-electrode potentiostat setup connected to an electrochemical analyzer (Model 660E, CH Instruments). The Fluorine tin oxide conductive glass (FTO) glass of 1 × 2 cm in size was covered with photocatalyst that was achieved by first mixing a catalyst (3-5 mg) in naphthol solution (20 μL) and chitosan solution (3 mL) under the action of 40 kHz ultrasonic wave for 1 h and then covering on FTO by spin coater, followed by drying at room temperature and further drying at 40 °C overnight in a vacuum oven. The area of the photoelectrode was controlled to be 1 cm^2.

The photoelectrochemical system consisted of an FTO glass covered by the photocatalyst, a coiled Pt wire, and a saturated Ag/AgCl/KCl (saturated) electrode as the working, counter, and reference electrode, respectively. The photocurrent was collected at 0.9 V versus NHE (0.6 V versus Ag/AgCl) in a Na_2SO_4 solution (0.5M, pH 6.9). Electrochemical impedance spectroscopy analysis was performed at a D.C. voltage of −0.5 V versus Ag/AgCl with an A.C. voltage amplitude of 5 mV in a frequency range from 100 kHz to 0.1 Hz. For the Mott–Schottky measurements, a similar strategy was performed on FTO glass (1 × 2 cm) by the same doctor blade method. The area of the electrode for the Mott–Schottky measurements was controlled to be 1 cm^2. Mott–Schottky measurements were performed at a potential range from 1.6 V to −0.9 V versus NHE, with an A.C. voltage amplitude of 5 mV and

in a fixed frequency of 3 kHz or 5 kHz. Each increase of potential is 0.05 V. The quiet time for each test is 2 s. The flat-band potential E_{FB} of the catalyst is calculated by the potential E_{SCE} measured by the reference electrode and its standard electrode potential E^{θ}_{SCE} according to Equation (1). For an n-type semiconductor, the conduction band bottom E_{CB} is 0.1-0.2V higher than E_{FB}, and then E_{CB} can be calculated according to Equation (2).

$$E_{FB} = E_{SCE} + E^{\theta}_{SCE} \text{ (vs. NHE)} \quad (1)$$

$$E_{CB} = E_{FB} - 0.10\text{V (vs. NHE)} \quad (2)$$

1.2 Detailed process for electrochemical tests using RDE

Cyclic voltammetry (CV) and linear sweep voltammetry (LSV) are tested with a three electrodes pyrex glass system, in which potassium chloride (KCl) saturated Ag/AgCl, Pt wire, and catalysts coated glassy carbon (GC) electrodes are used as the reference, counter, and working electrode, respectively. Ar and O_2 saturated 0.1 M KOH solutions are taken as electrolytes independently. Cyclic voltammetry (CV) and linear sweep voltammetry (LSV) are conducted with the help of Metrohm multi-Autolab M204 (CHI 660E) potentiostat/galvanostat. GC rotating disk electrode (RDE) from Pine Instrument is used to assess the ORR kinetics. The RDE experiments are performed on a 5.0 mm diameter GC E5 disk. All the potential values from CVs and LSVs measurements in the alkaline electrolyte are converted to the reversible hydrogen electrode (RHE) via the following Equation (3).

$$E_{RHE} = E_{Ag/AgCl} + 0.0591pH + {}^{0}E_{Ag/AgCl} = E_{Ag/AgCl} + 0.965 \quad (3)$$

Where $E^{0}_{Ag/AgCl}$ = 0.1976 V (25 °C). The number of electrons (n) associated with the ORR is evaluated from the Koutecky-Levich (K-L) analysis shown in Fig. 8a. K-L equation (4) is used to estimate the n.

$$\frac{1}{j} = \frac{1}{j_k} + \frac{1}{B\omega^{0.5}} \quad (4)$$

Here j and j_k are the total current density and kinetic current density, respectively, and ω is the angular velocity in rotation per minute (rpm), and B is the Levich slope, which is estimated as follows equation (5).

$$B = 0.201nFC_{O_2}D_{O_2}^{2/3}\upsilon^{-1/6} \quad (5)$$

Where n represents the transferred electron number, F is the Faraday constant (F = 96485 C mol^{-1}), D_{O_2} is the diffusion coefficient of O_2 in 0.1 mol L^{-1} KOH (1.9×10^{-5} cm^2 s^{-1}), υ is the kinetic viscosity (0.01 cm^2 s^{-1}), and C_{O_2} is the bulk concentration of O_2 (1.2×10^{-7} mol·cm^{-3}).

The voltammograms were measured in an O_2-saturated aqueous 0.1 M KOH (25℃) at 5 mV·s^{-1} with various rotating rates (400, 900, 1600, 2500 rpm). The working electrode is prepared as follows [S1]: 5 mg of the synthesized composite solid is added in 1 mL ethanol and ultrasonicated for 30 min. Afterward, 50 uL of Nafion solution (5 wt %) is mixed and sonicated for another 30 min. After that, 20 uL of the resultant solution is drop cast onto a glassy carbon (GC) electrode and thoroughly dried. The catalyst loading is 385 μg cm^{-2}.

2 Detailed experimental process

2.1 Preparation of dihydropyridine ACMD and its structural characterization data

P-hydroxybenzaldehyde, malononitrile, ammonium acetate, ethyl acetoacetate, triethylamine phosphate, and nano TiO_2 were all purchased from McLean and Aladdin Biochemical Technology Co., Ltd. these materials are analytical pure and used directly.

Synthesis of intermediate 2-(4-hydroxy benzylidene)propionitrile. In a flask, 2 g (16.38 mmol） of p-hydroxybenzaldehyde, 1.08 g (16.35 mmol）of propionitrile, and 15 mL of ethanol were added and stirred at room temperature for about 2 h to form yellow solid precipitation. Then the solid was filtered, rinsed with deionized waters (2×10 mL), and then dried at 60℃ to obtain 2.61g (15.35 mmol） the targeted intermediate, yellow solid, yield 95%, M.P. 186 ℃. FT-IR (cm-1, KBr) :3350.99, 2351.97, 2227.66, 1571.59, 1295.27, 1170.62, 833.61, 635.02.

Synthesis of ACMD. Because of the low efficiency of literature methods, we adopted a new catalytic synthesis to obtain ACMD [S2-S4]. In a flask, 0.5 g (2.94 mmol) 2-(4-hydroxy benzylidene)malononitrile, 0.32 g (7.14 mmol) ammonium acetate, 0.55 g (4.23 mmol) ethyl acetoacetate, and 0.1 g (0.5 mmol) catalyst triethylamine phosphate were mixed and added to 5 mL ethanol, then the solution was maintained at about 30 ℃ with stirring to react for about 4 h. After the completion of cyclo-condensation reaction (monitored by TLC), 2 mL water was added to promote

the precipitation of product, and then crude ACMD was obtained through vacuum filtration and drying at 60℃ for 8 h. After recrystallization with ethanol, the earthy yellow ACMD was obtained in 60% yield, M.P. 143 ℃. FT-IR (cm^{-1}, KBr) :3390.54, 3327.66, 3207.49, 2983.70, 2934.56, 2198.38, 1701.48, 1222.37. ^{1}H NMR (400 MHz, DMSO-d_6, Fig.S1) δ (ppm): 9.32 (s, 1H, -NH),9.31 (s, 1H, Ar-OH), 6.95 – 6.80 (m, 4H, Ar-H), 6.70 – 6.63 (m, 2H, -NH_2), 4.16 (d, J = 0.6 Hz, 1H, -CH), 4.06 – 3.87 (m, 2H, -CH_2-O), 2.26 (d, J = 0.6 Hz, 3H, Me), 1.04 (t, J = 7.1 Hz, 3H, Ar-CH_3).

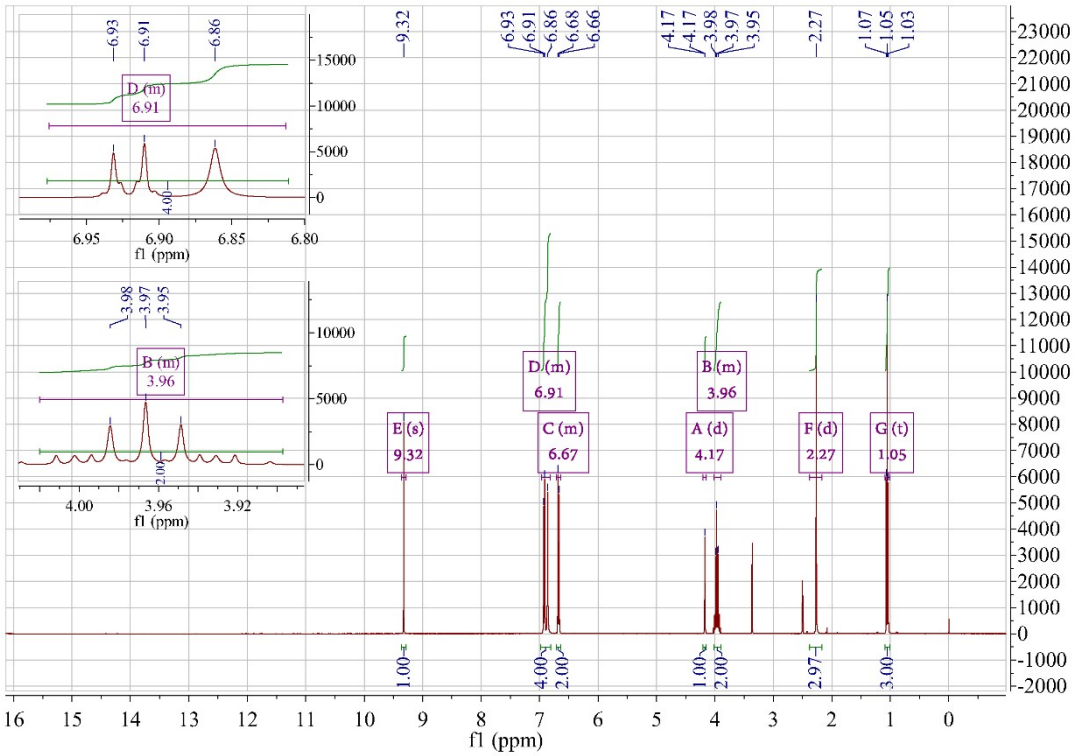

Fig.S1 ^{1}H NMR of ACMD

2.2 Determination of quantum efficiency and solar energy efficiency

2.2.1 Apparent quantum efficiency analysis

The measurement of apparent quantum efficiency (AQE) was carried out in a

quartz reactor. As a typical run, 10 mL of pure water, 10 mg of catalysts, and 500 μL Benzyl alcohol were added into the reactor. After 10 min of ultra-sonication and O_2 bubbling, it was irradiated by a Xenon lamp (GX2300, equipped with light filters 365±5 nm and 435±10 nm) for 6 h. The average intensities of irradiation to the reactor were determined by a spectroradiometer (PL-MW2000). The AQE was calculated using the following equation:

$$AQY = \frac{N_e}{G_p} \times 100\%$$

Where the reaction electrons amount, N_e was determined by the following equation:

$$N_e = 2 \times n \times N_A$$

The incident photon quantity (G_p) was determined by the following equation:

$$G_p = \frac{1}{hc}\int_{\lambda_1}^{\lambda_2} G_e(\lambda)\lambda d\lambda$$

Where the functional relation of energetic quantity $G_e(\lambda)$ and wavelength λ was determined by the numerical simulation of the energy distribution of xenon lamp in the transmission band. Then AQE was obtained under the known data, including the amount of H_2O_2 molecules (n), the Avogadro constant (N_A), the speed of light (c), and the Planck constant (h).

2.2.2 Determination of solar-to-chemical conversion efficiency.

Solar-to-chemical conversion efficiency (SCC) was determined by a 300 W xenon solar simulator, and a light-blocking plate with a hole of 2cm diameter is placed in the front to control the light-receiving area of the reaction solution. The

photoreaction was performed in pH = 2 solution (100 mL) with photocatalyst (50 mg) under O_2 bubbling in a jacketed beaker equipped with a light filter. Before the photo reaction, the solution was stirred in dark for 1h to balance the adsorption, and after light radiation started, 1 mL sample solution was taken out every 2h to determine H_2O_2 concentration. Then, the SCC of the catalyst was calculated by the following equation:

$$SCC(\%) = \frac{\Delta G \cdot n}{E \cdot t} \times 100\%$$

where ΔG is the free energy for H_2O_2 generation (117 kJ mol^{-1}), n is the amount of H_2O_2 formed (mol), t is the irradiation time (s), and E is the total input power (W). The overall irradiation intensity of the AM1.5 global spectrum (300-2,500 nm) is 1,000 W m^{-2}, and the irradiation area is 3.14×10^{-4} m^2, the total input power over the irradiation area is thus determined to be 0.314 W.

2.3 H_2O_2 degradation study

To determine the properties of catalyst-induced photodecomposition of H_2O_2, 10 mg of the photocatalyst was added into 10 mL of 27.6 mM H_2O_2 aqueous solution containing 500 μL benzyl alcohol and 1 mmol Na_2SiO_3. After ultrasonic dispersion for 5 min, it was kept in dark for 30 min to make it reach adsorption equilibrium. Then, photosynthesis was conducted with the irradiation of a xenon lamp (300 W, > 300 nm), and the samples were taken out every 1h. TiO_2 as a reference is determined according to the same process.

2.4 Effect of benzyl alcohol on the reaction

In the reaction tube, 10 mg catalyst, 10 mL H_2O, and 500 μL benzyl alcohol were added and ultrasonically dispersed for 5 min and maintained in dark for 30 min with stirring, and then the photocatalytic reaction was carried out under the bubbling of O_2 and N_2 respectively. Samples were taken every 2 h to analyze the concentration of H_2O_2. Under the same conditions, the comparative experiments were conducted without adding benzyl alcohol, to test the concentration of H_2O_2 obtained by bubbling O_2 and N_2 respectively. The results are illustrated in **Fig.S4**.

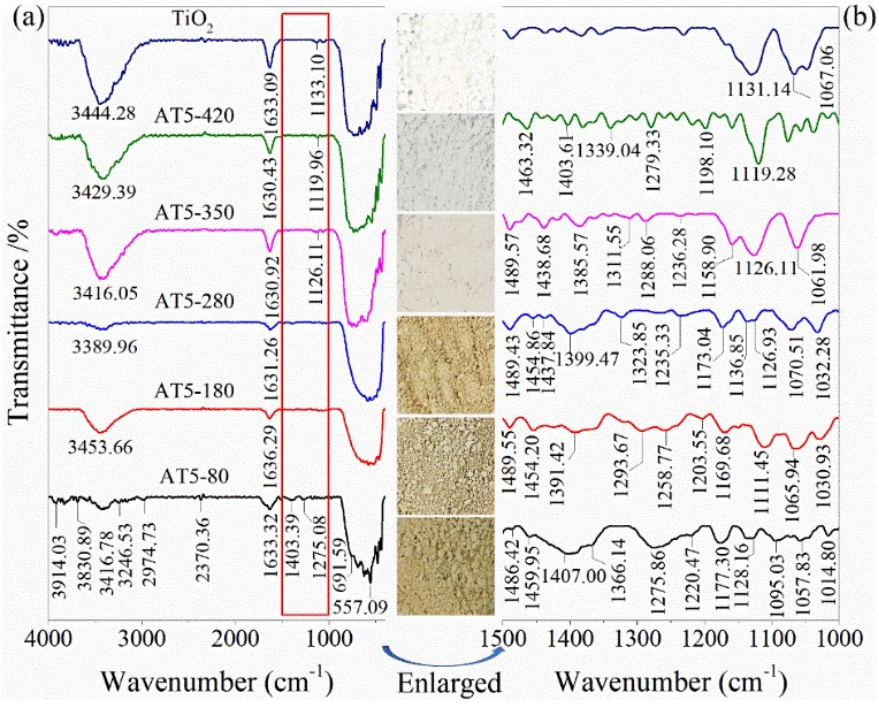

Fig.S2 FT-IR spectra of the catalyst ACMD-TiO_2 calcined at different temperatures (a) and their enlarged view of the part between 1000-1500cm^{-1} (b). The inserted pictures between them are the appearance of the corresponding catalyst.

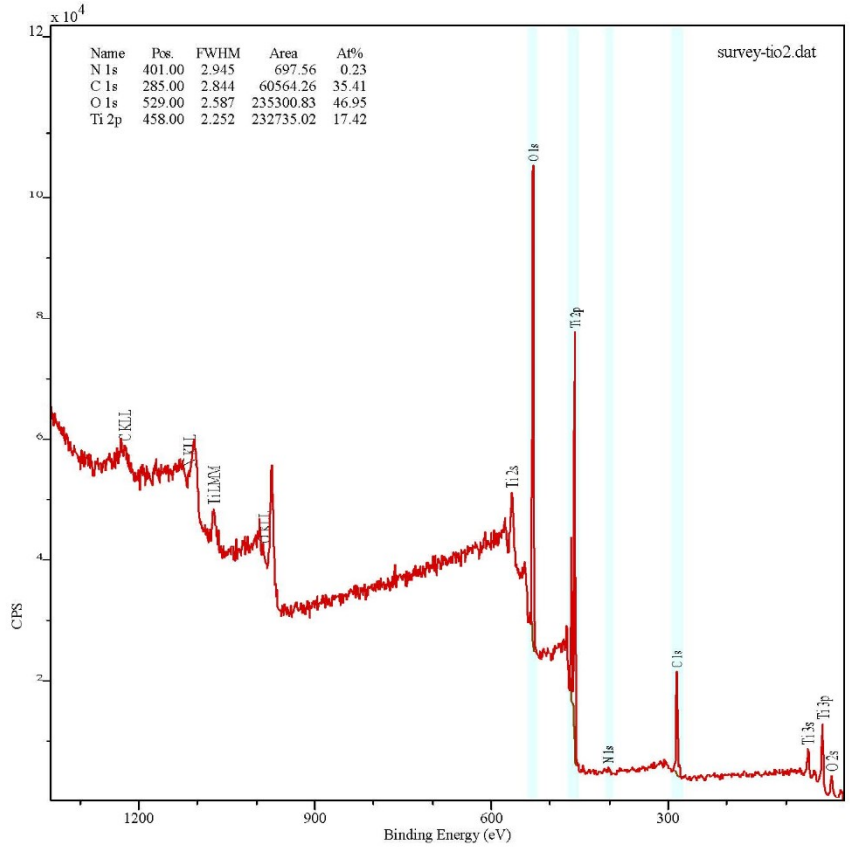

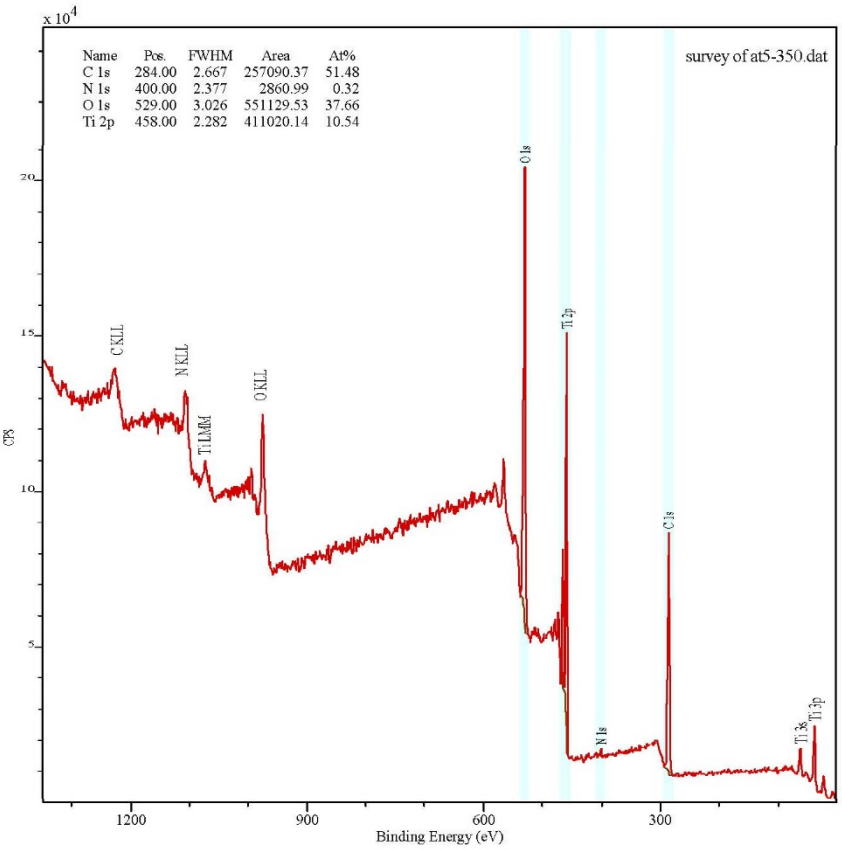

Fig.S3 Elements content of TiO_2 and AT5-350

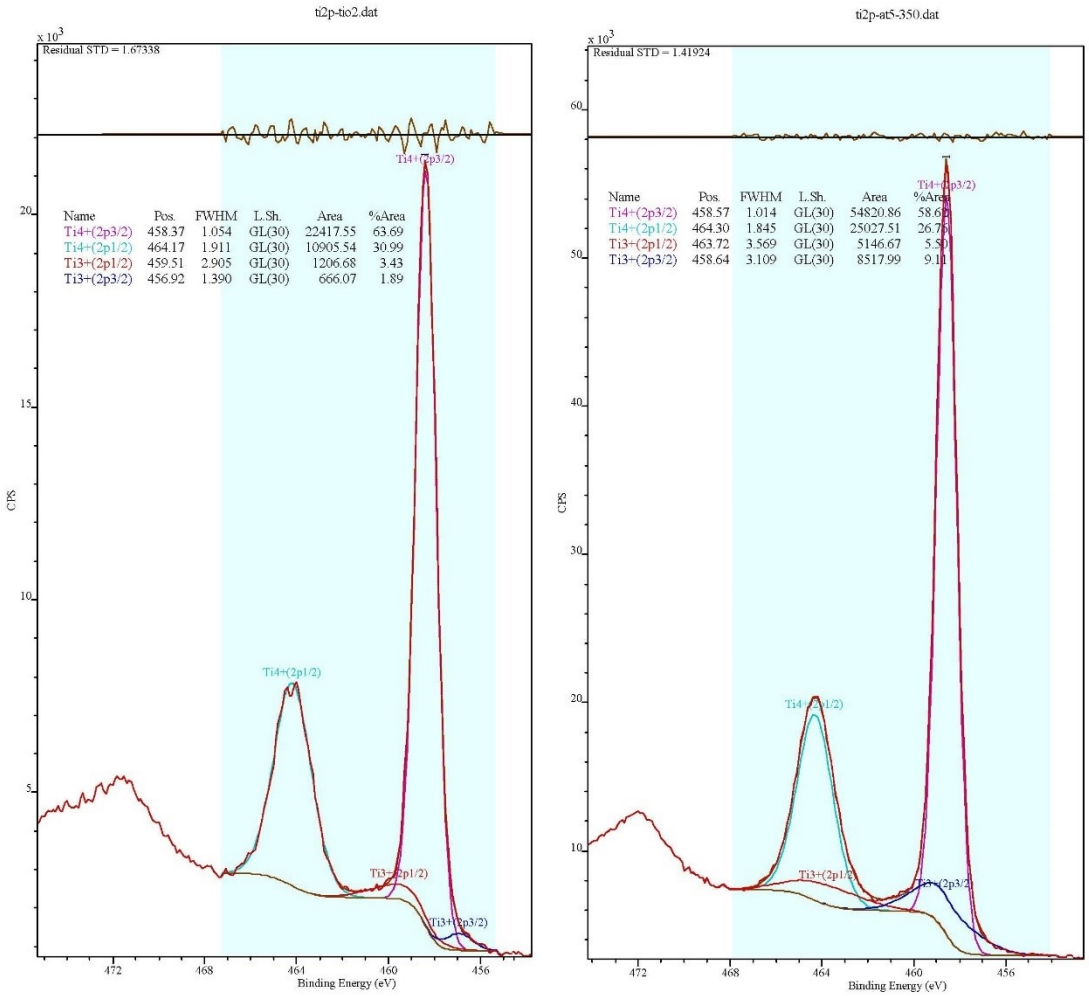

Fig.S4 High-resolution XPS spectra of Ti2p for TiO_2 (left) and AT5-350 (right)

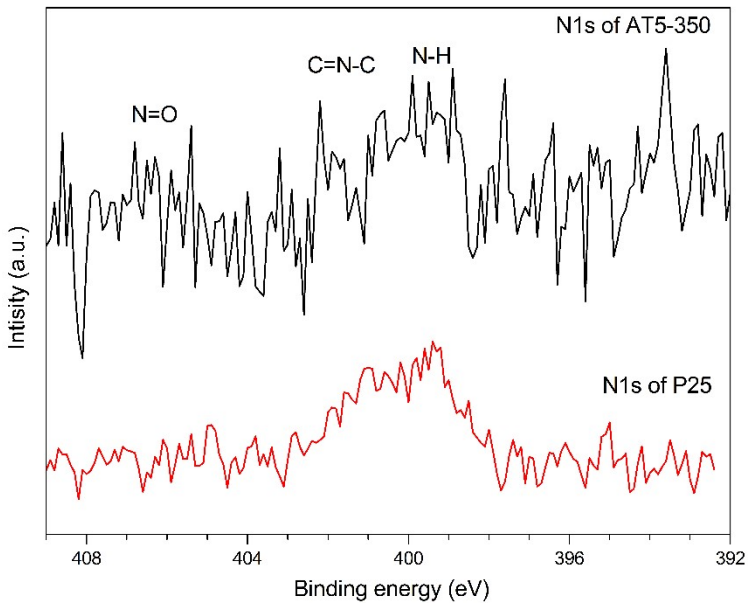

Fig.S5 High-resolution XPS spectra of N1s for TiO_2 and AT5-350

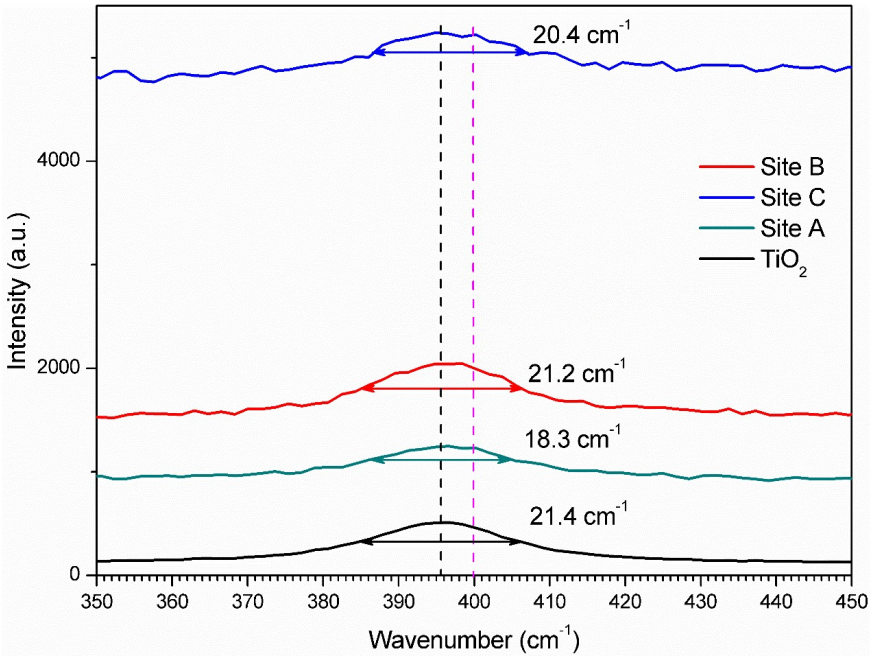

Fig.S6 Raman mode of $B_{1g}(1)$ for TiO_2 and different sites of ACMD-TiO_2 marked with FWHM.

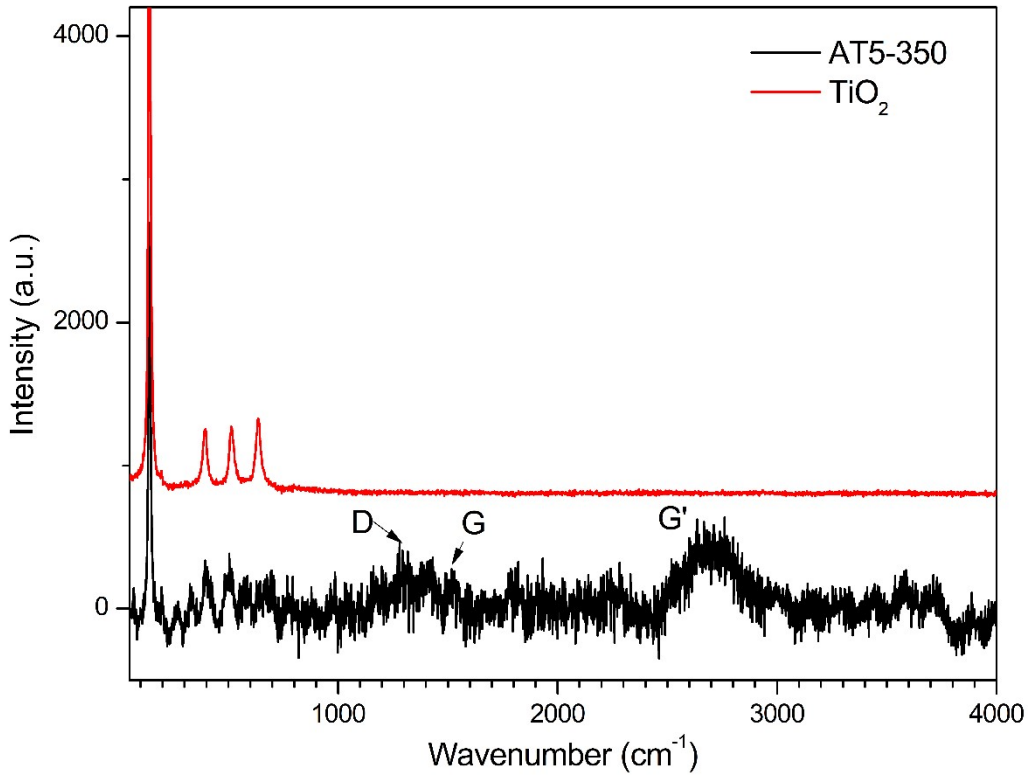

Fig.S7. Raman spectra of TiO_2 and AT5-350 under 785 nm laser

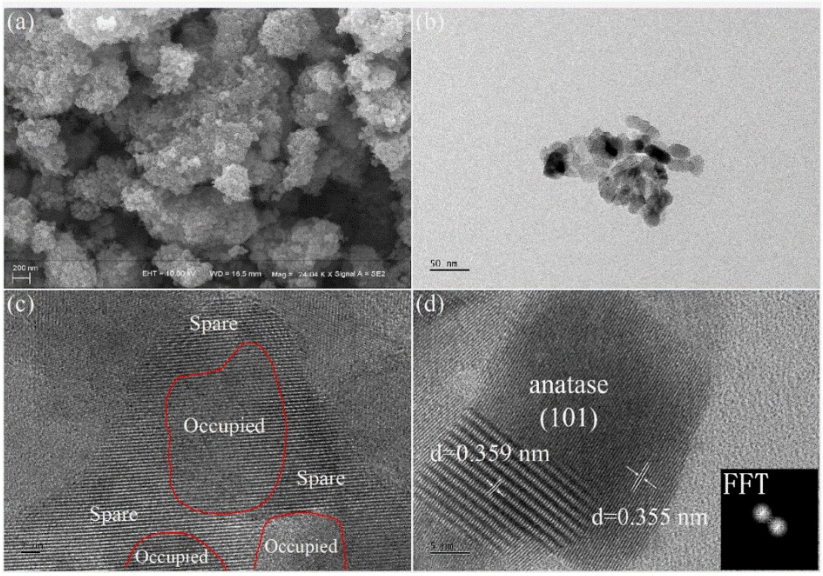

Fig.S8. Surface features of ACMD-TiO_2. (a) HRSEM, (b) and (c) HRTEM features. (d) diffraction and FFT of the HRTEM feature (The inserted is the FFT photo).

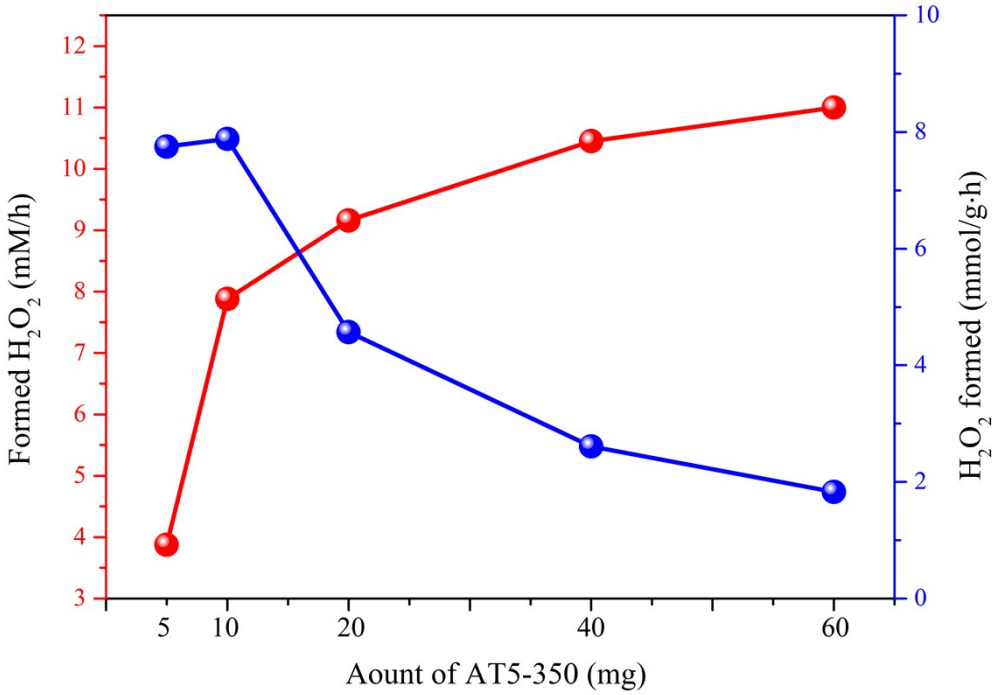

Fig.S9 The influence of AT5-350 amount on H_2O_2 production.

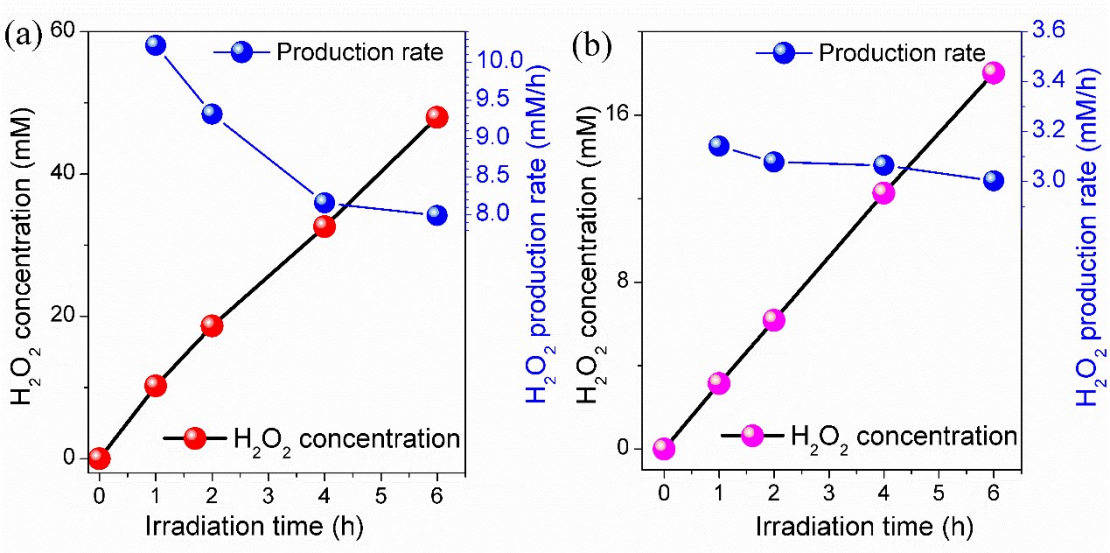

Fig.S10 Comparison of H_2O_2 production under different irradiation of xenon light (a) above 300 nm and (b) above 420 nm.

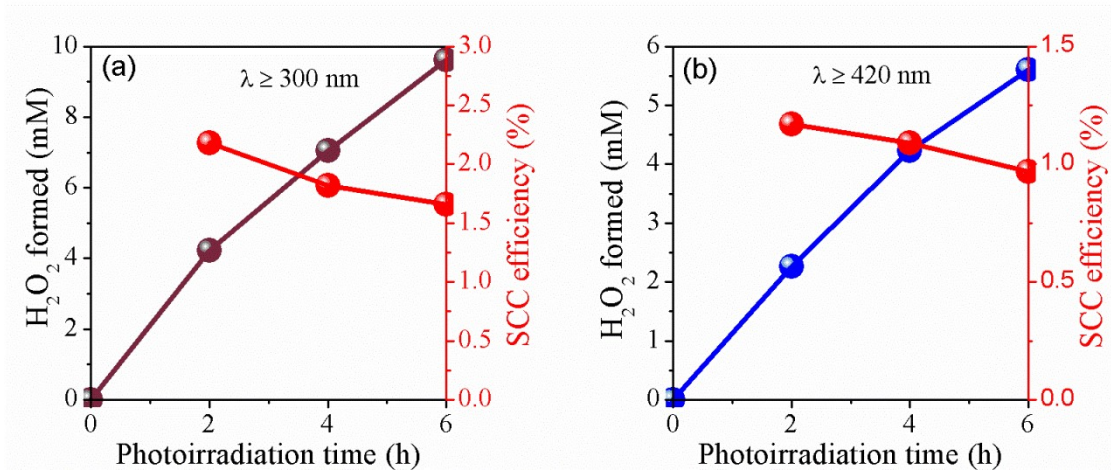

Fig.S11 SCC efficiency of catalyst AT5-350 under visible light irradiation. (Conditions: 10 mg catalyst and 500 μL benzyl alcohol were used in 10 mL water, pH = 2, Xenon lamp 300W, > 420 nm)

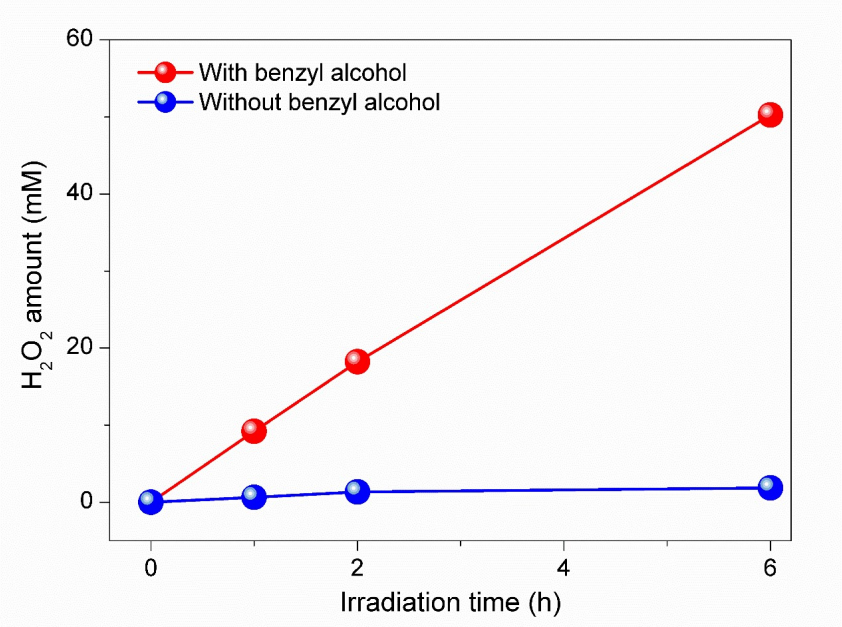

Fig.S12 H_2O_2 formed by bubbling O_2 and N_2 with or without benzyl alcohol

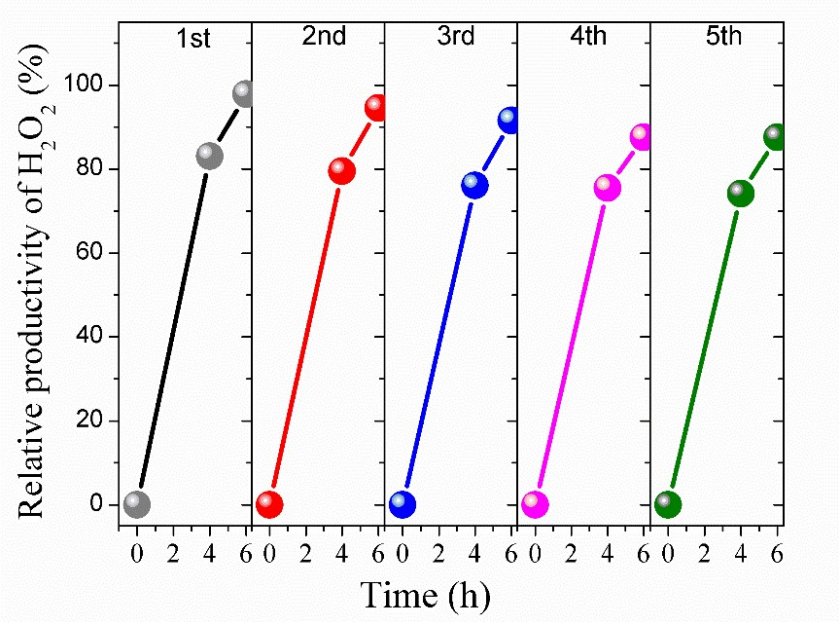

Fig.S13 Relative productivity of H_2O_2 in each reuse run (Conditions: 10 mg catalyst and 500 μL benzyl alcohol were used in 10 mL water, pH = 2, Xenon lamp 300W, > 300 nm).

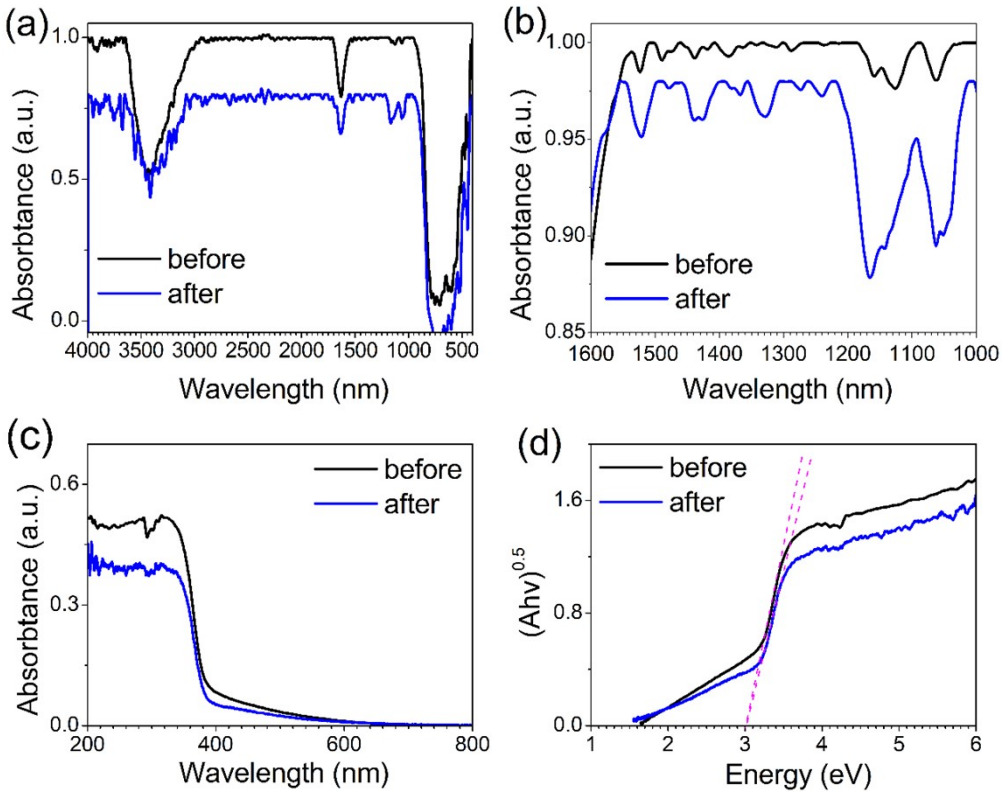

Fig.S14 Structural comparison of catalyst AT5-350 before and after reuse 5 times. (a) Full FTIR spectra, (b) Enlarged FTIR view of 1600-1000cm^{-1}, (c) UV-vis DRS, and (d) Tauc plots.

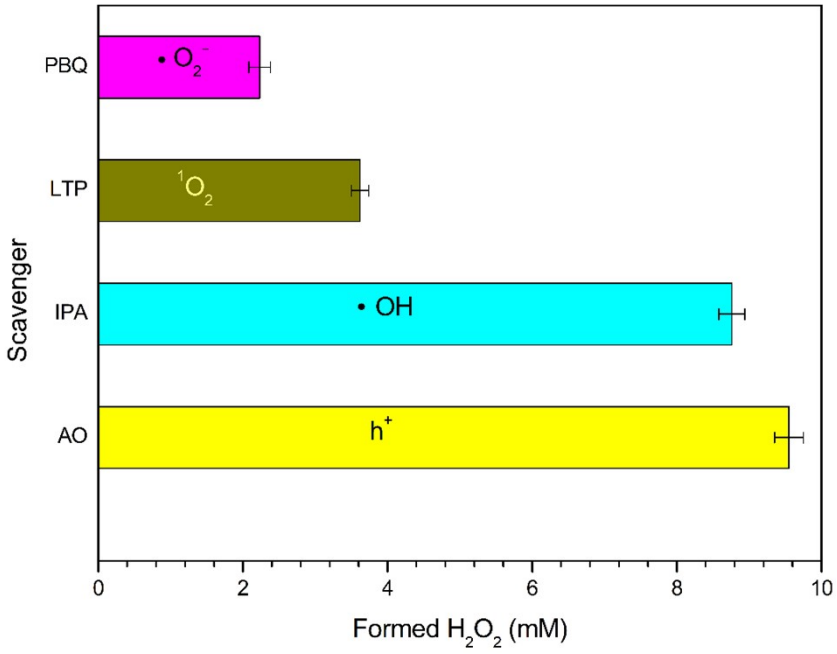

Fig.S15 Scavenger test results of catalyst AT5-350. Conditions: 10 mg catalyst and 500 μL benzyl alcohol were used in 10 mL water with pH = 2, and 0.01M scavenger was used in 10 mL reactant, irradiating with 300W Xenon lamp (> 300 nm) for 2 h.

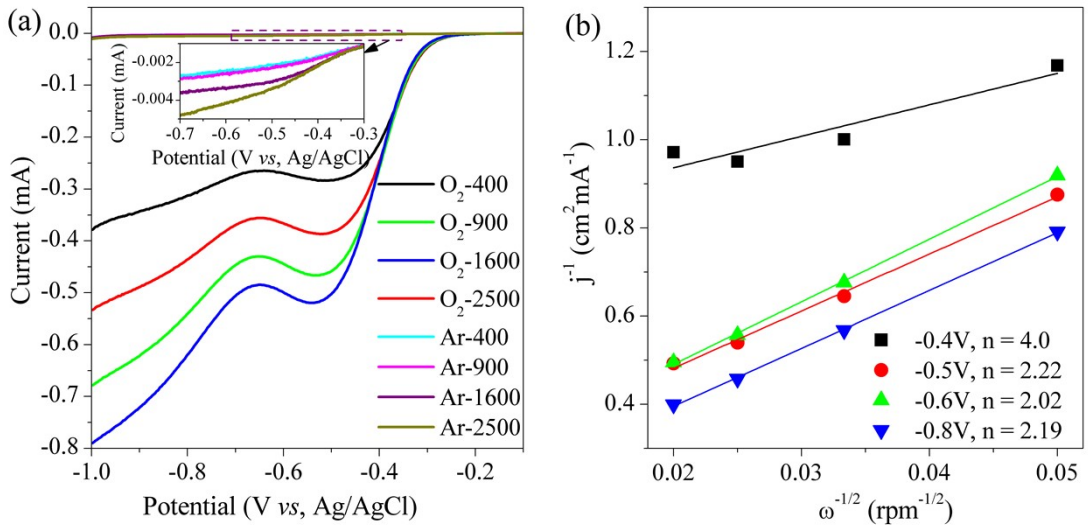

Fig.S16 (a) Linear-sweep voltammograms of the catalyst AT5-350 and (b) The Koutecky–Levich plots at different potentials

Table S1 Graphitization reaction conditions of ACMD-TiO_2

Entry	ACMD amount (g/2g TiO_2)*	Temperature （℃）	Time （h）	Ventilation types	C(H_2O_2) (mM)**
1	0.05	180	2	O_2	15.12
2	0.05	280	3.5	/	28.19
3	0.05	380	5	Air	34.73
4	0.1	180	3.5	Air	19.22
5	0.1	280	5	O_2	22.04
6	0.1	380	2	/	30.75
7	0.2	180	5	/	6.92
8	0.2	280	2	Air	9.23
9	0.2	380	3.5	O_2	29.21
Mean value1	26.013	13.753	18.367	22.123	-
Mean value2	24.003	19.820	25.540	21.953	-
Mean value3	15.120	31.563	21.230	21.060	-
Range	10.893	17.810	7.173	1.063	-

* The dosage of TiO_2 is set as 2 g for each proportioning case.

**Using 10 mg catalyst in 10 mL water with 500 μL benzyl alcohol, air bubbling to provide oxygen, and irradiated with 300 W xenon lamp for 6 h.

Table S2 The results of further optimization for the conditions of ACMD-TiO_2

Entry	ACMD amount (g)*	Temperature (℃)	$C(H_2O_2)$ (mM)**
1	0.05	320	20.66
2	0.05	350	37.26
3	0.05	380	30.81
4	0.05	420	33.57
5	0.1	320	28.34
6	0.1	350	40.00
7	0.1	380	35.11
8	0.1	420	24.86

* The dosage of TiO_2 is set as 2 g for each proportioning case.

**Using 10 mg catalyst in 10 mL water with 500 μL benzyl alcohol, air bubbling to provide oxygen, and irradiated with 300 W xenon lamp for 6 h.

Table S3 Comparison of H_2O_2 production.

Photocatalyst	Electron donor	Wavelength /nm	H_2O_2 /mmol/(h·g)	ϕ_{AQY} /%	Ref.
Au-Ag/TiO_2	Ethanol	>280	0.15	—	[S5]
TiO_2	Benzyl alcohol	>280	0.33	29.1@334 nm [a]	[S6]
Au/TiO_2	HCOOH	>420	0.64-0.70	13.7@450 nm	[S7]
Si/TiO_2-Au(electrode)	/	365	5.7uM/h [b]	—	[S8]
CoPi/rGO/TiO_2	2-propanol	≥320	3	—	[S9]
TiO_2/rGO/Carbon dots	2-propanol	AM1.5	0.35	—	[S10]
TiO_2/WO_3/rGO	2-propanol	AM1.5	0.27	—	[S11]
Au/TiO_2	C2H5OH	>320	0.625	—	[S12]
SN-GQD/TiO_2	2-propanol	>420	0.902	—	[S13]
TiO_2	2-propanol	=365	0.2116	19.8@365 nm	[S14]
Au/TiO_2	CH3OH	>320	0.35	—	[S15]
Co@TiO_2	CH3OH	=400	1.7	—	[S16]

HTNT-CD	Ethanol	>420	3.42	5.2@365 nm	[S17]
SNG/TiO_2	2-propanol	≥300	0.0746	—	[S18]
Au/SnO_2-TiO_2	Alcohol	UV	0.6	—	[S19]
Pt-TiO_2	/	Full	5.096	—	[S20]
Carbon/Au-TiO_2	EtOH	=367	3.69	17.29@367 nm	[S21]
Au/[SnO_2−NR#TiO_2]	EtOH	420-485	0.01	—	[S22]
Au/Bi_2O_3-TiO_2	EtOH	>420	0.93	—	[S23]
RuO_2#TiO_2–Au	/	>300	0.08	—	[S24]
TNS	ethanol	>300	1.746	5.96@365 nm [a]	[S25]
TiO_2/Pt/Co POM	methanol	=365	1.395	1.09@365 nm [a]	[S26]
Cu^{2+}/TiO_2	/	=300-400	9.6×10^{-4}	—	[S27]
F-TiO_2	HCOOH	=360	0.96-1.25	—	[S28]
Zn^{2+}/TiO_2	/	125W Hg	0.15	—	[S29]
Au/TiO_2	Ethanol	>300	0.25	13@355±23 nm [a]	[S30]
ACMD- TiO_2	Benzyl alcohol	>300	10.22	24.5@365nm[a]	This work

[a] AQE

[b] Weight of electrode made of catalyst not provided.

3. Statement about Tauc efficiency

It should be noted that there are many factors affecting the modes of electronic transition energy (direct and indirect), such as band alignments and surface electronic states of each TiO_2 phase, which all are based on the preparation and the formation of TiO_2. For this reason, for this report, the *Eg* of all as-modified TiO_2 was mainly related to the indirect transition and thus Tauc efficiency 2 was used to determine it.

References

[S1] D. Mahato, Y. P. Kharwar, K. Ramanujam, P. Haridoss, T. Thomas, *Int. J. Hydrogen Energy* **2021**, *46*, 21549–21565. https://doi.org/10.1016/j.ijhydene.2021.04.013.

[S2] J. Marco-Contelles, R. León, C. De Los Ríos, A. Samadi, M. Bartolini, V. Andrisano, O. Huertas, X. Barril, F. J. Luque, M. I. Rodríguez-Franco, B. López, M. G. López, A. G. García, M. D. C. Carreiras, M. Villarroya, *J. Med. Chem.* **2009**, *52*, 2724–2732. https://doi.org/10.1021/jm801292b.

[S3] S. Khot, P. B. Auti, S. A. Khedkar, *Mini-Reviews Med. Chem.* **2020**, *21*, 135–149. https://doi.org/10.2174/1389557520666200807130215.

[S4] J. Safaei-Ghomi, A. Ziarati, R. Teymuri, *Bull. Korean Chem. Soc.* **2012**, *33*, 2679–2682. https://doi.org/10.5012/bkcs.2012.33.8.2679.

[S5] D. Tsukamoto, A. Shiro, Y. Shiraishi, Y. Sugano, S. Ichikawa, S. Tanaka and T. Hirai, *ACS Catal.*, 2012, **2**, 599–603. doi: 10.1021/cs2006873.

[S6] Y. Shiraishi, S. Kanazawa, D. Tsukamoto, A. Shiro, Y. Sugano, T. Hirai, *ACS Catal.* **2013**, *3*, 2222–2227. https://doi.org/10.1021/cs400511q.Y

[S7] Y. Shiraishi, S. Kanazawa, Y. Kofuji, H. Sakamoto, S. Ichikawa, S. Tanaka and T. Hirai, *Angew. Chemie*, 2014, **126**, 13672–13677. doi: 10.1002/ange.201407938.

[S8] N. Kaynan, B. A. Berke, O. Hazut and R. Yerushalmi, *J. Mater. Chem. A*, 2014, **2**, 13822–13826. doi: 10.1039/c4ta03004d.

[S9] G. H. Moon, W. Kim, A. D. Bokare, N. E. Sung and W. Choi, *Energy Environ. Sci.*, 2014, **7**, 4023–4028. doi: 10.1039/c4ee02757d.

[S10] X. Zeng, Z. Wang, N. Meng, D. T. McCarthy, A. Deletic, J. hong Pan and X. Zhang, *Appl. Catal. B Environ.*, 2017, **202**, 33–41. doi: 10.1016/j.apcatb.2016.09.014.

[S11] X. Zeng, Z. Wang, G. Wang, T. R. Gengenbach, D. T. McCarthy, A. Deletic, J. Yu and X. Zhang, *Appl. Catal. B Environ.*, 2017, **218**, 163–173. doi: 10.1016/j.apcatb.2017.06.055.

[S12] M. Teranishi, S. I. Naya and H. Tada, *J. Phys. Chem. C*, 2016, **120**, 1083–1088. doi: 10.1021/acs.jpcc.5b10626.

[S13] L. Zheng, H. Su, J. Zhang, L. S. Walekar, H. Vafaei Molamahmood, B. Zhou, M. Long and Y. H. Hu, *Appl. Catal. B Environ.*, 2018, **239**, 475–484. doi: 10.1016/j.apcatb.2018.08.031.

[S14] B. O. Burek, D. W. Bahnemann and J. Z. Bloh, *ACS Catal.*, 2019, **9**, 25–37. doi: 10.1021/acscatal.8b03638.

[S15] X. Xiong, X. Zhang, S. Liu, J. Zhao and Y. Xu, *Photochem. Photobiol. Sci.*, 2018, **17**, 1018–1022. doi: 10.1039/c8pp00177d.

[S16] T. Baran, S. Wojtyła, A. Minguzzi, S. Rondinini and A. Vertova, *Appl. Catal. B Environ.*, 2019, **244**, 303–312. doi: 10.1016/j.apcatb.2018.11.044.

[S17] R. Ma, L. Wang, H. Wang, Z. Liu, M. Xing, L. Zhu, X. Meng and F. S. Xiao, *Appl. Catal. B Environ.*, 2019, **244**, 594–603. doi: 10.1016/j.apcatb.2018.11.087.

[S18] L. Zheng, J. Zhang, Y. H. Hu and M. Long, *J. Phys. Chem. C*, 2019, **123**, 13693–13701. doi: 10.1021/acs.jpcc.9b02311.

[S19] G. Zuo, B. Li, Z. Guo, L. Wang, F. Yang, W. Hou, S. Zhang, P. Zong, S. Liu, X. Meng, Y. Du, T. Wang and V. A. L. Roy, *Catalysts*, 2019, **9**, 623. DOI:10.3390/catal9070623.

[S20] L. Wang, S. Cao, K. Guo, Z. Wu, Z. Ma and L. Piao, *Chinese J. Catal.*, 2019, **40**, 470–475. doi: 10.1016/s1872-2067(19)63274-2.

[S21] Z. Liu, X. Sheng, D. Wang and X. Feng, *iScience*, 2019, **17**, 67–73. doi: 10.1016/j.isci.2019.06.023.

[S22] K. Awa, S. I. Naya, M. Fujishima and H. Tada, *J. Phys. Chem. C*, 2020, **124**, 7797–7802. doi: 10.1021/acs.jpcc.9b11875.

[S23] L. Feng, B. Li, Y. Xiao, L. Li, Y. Zhang, Q. Zhao, G. Zuo, X. Meng and V. A. L. Roy, *Catal. Commun.*, 2021, **155**, 0–3, DOI:10.1016/j.catcom.2021.106315.

[S24] M. Nagamitsu, K. Awa and H. Tada, *Chem. Commun.*, 2020, **56**, 8190–8193. doi: 10.1039/d0cc03327h.

[S25] Y. Yang, B. Zhu, L. Wang, B. Cheng, L. Zhang and J. Yu, *Appl. Catal. B Environ.*, 2022, **317**, 121788. DOI:10.1016/j.apcatb.2022.121788.

[S26] B. He, C. Luo, Z. Wang, L. Zhang and J. Yu, *Appl. Catal. B Environ.*, 2023, **323**, 122200. DOI:10.1016/j.apcatb.2022.122200.

[S27] R. Cai, Y. Kubota and A. Fujishima, *J. Catal.*, 2003, **219**, 214–218. doi: 10.1016/S0021-9517(03)00197-0.

[S28] V. Maurino, C. Minero, G. Mariella and E. Pelizzetti, *Chem. Commun.*, 2005, 2627–2629. doi: 10.1039/b418789j.

[S29] V. Maurino, C. Minero, E. Pelizzetti, G. Mariella, A. Arbezzano and F. Rubertelli, *Res. Chem. Intermed.*, 2007, **33**, 319–332. doi: 10.1163/156856707779238711.

[S30] M. Teranishi, S. I. Naya and H. Tada, *J. Am. Chem. Soc.*, 2010, **132**, 7850–7851. doi: 10.1021/ja102651g.